Med. Biol. Eng. Comput. manuscript No.
(will be inserted by the editor)

Mark Potse · **Bruno Dubé** · **Alain Vinet**

Cardiac Anisotropy in Boundary-Element Models for the Electrocardiogram

Date: 2009/01/21 14:03:34 Revision: 1.110

Computational resources for this work were provided by the Réseau québécois de calcul de haute performance (RQCHP). M. Potse was supported by the Research Center of Sacré-Coeur Hospital, Montreal, Quebec, Canada.

M. Potse · B. Dubé · A. Vinet

Research Center, Sacré-Coeur hospital

5400 Boulevard Gouin Ouest

Montreal, Quebec H4J 1C5

Canada

Tel.: +1 514 338-2222 ext. 2519

Fax: +1 514 338-2694

E-mail: mark@potse.nl

E-mail: bruno.dube@umontreal.ca

E-mail: alain.vinet@umontreal.ca

M. Potse

Interuniversity Cardiology Institute of The Netherands

Utrecht, The Netherlands; and

Laboratory for Experimental Cardiology

Heart Failure Research Center

Academic Medical Center

Amsterdam, The Netherlands

Abstract The boundary-element method (BEM) is widely used for electrocardiogram (ECG) simulation. Its major disadvantage is its perceived inability to deal with the anisotropic electric conductivity of the myocardial interstitium, which led researchers to represent only intracellular anisotropy or neglect anisotropy altogether. We computed ECGs with a BEM model based on dipole sources that accounted for a "compound" anisotropy ratio. The ECGs were compared with those computed by a finite-difference model, in which intracellular and interstitial anisotropy could be represented without compromise. For a given set of conductivities, we always found a compound anisotropy value that led to acceptable differences between BEM and finite-difference results. In contrast, a fully isotropic model produced unacceptably large differences. A model that accounted only for intracellular anisotropy showed intermediate performance. We conclude that using a compound anisotropy ratio allows BEM-based ECG models to more accurately represent both anisotropies.

Keywords myocardial anisotropy · boundary-element methods · finite-difference model · electrocardiogram · computer model

1 Introduction

The electrocardiogram (ECG) is arguably the most important diagnostic tool in cardiology. Although it has been around for more than a century, many aspects of the ECG are still poorly understood. Computer models of the ECG play an important role in filling these knowledge gaps. Whole-heart reaction-diffusion models, which can simulate the ECG directly from processes on the membrane level, have only just begun to appear [21, 24, 25, 51]. These models, combined with patient-specific anatomic models, can predict subtle electrocardiographic effects of ion-channel malfunctions, provided that the ECG simulation is accurate enough.

The boundary-element method (BEM) has been used for ECG simulation for more than four decades [1, 3, 9, 16, 19, 21, 28, 32, 47, 55]. Its attractiveness comes from the small number of surface elements necessary to describe the torso and its major inhomogeneities. The torso, skeletal muscle layer, lungs, and ventricular blood masses can be modeled with a few thousand triangles [16]. Originally the small footprint of the BEM model made it the only candidate for ECG simulation [16, 19, 32]. The continuing popularity of the method is mainly due to its speed, which makes it useful for low-end computers and interactive applications [37].

The BEM is used to model the conductivity of the torso components. It is combined with a source model, which represents the cardiac electrical activity. The source model can be a small number of dipole sources inside the myocardium [16, 19, 32, 52], which can be computed from membrane potentials simulated by a reaction-diffusion model [51] or by simpler models [28]. Other source models are the “uniform-” or “oblique dipole layer” on the activation front [6, 7, 42] and the “equivalent double layer” on the surface of the myocardium [11, 35, 36]. We will discuss only dipole sources.

The major disadvantage of the BEM model for ECG simulation is its inability to represent the anisotropy of the extracellular space in the cardiac muscle. Both intracellular and extracellular anisotropy affect the ECG. Intracellular anisotropy can be treated straightforwardly, as has been done in several studies [20, 53]. However, when extracellular anisotropy is neglected, the effect of intracellular anisotropy in the model is exaggerated. Because of this, previous authors have expressed doubt as to whether such models should represent intracellular anisotropy [14, 50]. Many models neglected anisotropy completely.

Anisotropy has important effects on the precordial ECG leads. For example, when subendocardial ischemia is modeled, the effect of anisotropy can make the difference between a positive and a negative ECG deflection [29], with important consequences for diagnosis. Thus, anisotropic ECG simulation can be important and the question is whether BEM models can reliably account for it.

The purpose of this study is to demonstrate that a good approximative treatment of extracellular anisotropy in a BEM model is possible, and that accounting for both anisotropies improves the simulated ECG. We compared ECGs computed by a BEM model with those computed by a finite-difference model, in which anisotropy could be represented without compromise.

2 Methods

Our methods are based on the bidomain model of cardiac tissue [14, 18, 32], which treats the myocardium as two continuous co-located media called the intracellular and extracellular domain, which are separated everywhere by the cell membrane. The conductivity in each domain is greater along than across the muscle fibers. We denote the fiber direction by a field of normalized row vectors $\hat{\mathbf{a}} = (a_x, a_y, a_z)$. The conductivity of each domain can then be characterized by a tensor field, generated by the function

$$\mathbf{G}(\sigma_\mathrm{L}, \sigma_\mathrm{T}) = \sigma_\mathrm{T}\mathbf{1} + (\sigma_\mathrm{L} - \sigma_\mathrm{T})\hat{\mathbf{a}}^\mathrm{T}\hat{\mathbf{a}} \tag{1}$$

where $\mathbf{1}$ is a unit tensor, and σ_L and σ_T are the conductivities parallel and perpendicular to the fiber axis, respectively [8]. Let σ_iL and σ_iT be the intracellular conductivities parallel and perpendicular to the fibers, respectively, and σ_eL and σ_eT their extracellular equivalents. We define the intracellular and extracellular conductivity tensors fields as $\mathbf{G}_\mathrm{i} = \mathbf{G}(\sigma_\mathrm{iL}, \sigma_\mathrm{iT})$ and $\mathbf{G}_\mathrm{e} = \mathbf{G}(\sigma_\mathrm{eL}, \sigma_\mathrm{eT})$. The anisotropy ratios of the two domains are $R_\mathrm{i} = \sigma_\mathrm{iL}/\sigma_\mathrm{iT}$ and $R_\mathrm{e} = \sigma_\mathrm{eL}/\sigma_\mathrm{eT}$. An overview of all conductivity values and anisotropy ratios is given in table 1.

Potential fields ϕ_i and ϕ_e in the two domains are related to current density fields $\mathbf{J}_\mathrm{i} = \mathbf{G}_\mathrm{i}\nabla\phi_\mathrm{i}$ in the intracellular domain and $\mathbf{J}_\mathrm{e} = \mathbf{G}_\mathrm{e}\nabla\phi_\mathrm{e}$ in the extracellular domain [14]. The divergence of each current density field equals the current that flows through the cellular membrane; this current must have equal magnitude and opposite sign in the two domains. Thus, the bidomain model can be summarized with the following equation [14, 18, 32]:

$$\nabla\cdot(\mathbf{G}_\mathrm{i}\nabla\phi_\mathrm{i}) = -\nabla\cdot(\mathbf{G}_\mathrm{e}\nabla\phi_\mathrm{e}) \tag{2}$$

It is convenient to use the transmembrane potential $V_\mathrm{m} = \phi_\mathrm{i} - \phi_\mathrm{e}$ to eliminate ϕ_i from equation (2); after-re-arranging terms we obtain an implicit equation for ϕ_e in terms of V_m:

$$\nabla\cdot([\mathbf{G}_\mathrm{i} + \mathbf{G}_\mathrm{e}]\nabla\phi_\mathrm{e}) = -\nabla\cdot(\mathbf{G}_\mathrm{i}\nabla V_\mathrm{m}). \tag{3}$$

In this study ECGs were simulated from given membrane potentials (V_m) by a BEM model and by a finite-difference (FD) model of the human torso. The FD model solved the extracellular potential ϕ_e from equation (3). The BEM model is conceptually more complicated. Its source model is an equivalent current density

$$\mathbf{J}_\mathrm{c} = -\mathbf{G}_\mathrm{c}\nabla V_\mathrm{m} \tag{4}$$

with $\mathbf{G}_\mathrm{c}$ a proposed "compound" conductivity tensor field

$$\mathbf{G}_\mathrm{c} = f_\mathrm{c}\mathbf{G}(R_\mathrm{c}\sigma_\mathrm{iT}, \sigma_\mathrm{iT}) \tag{5}$$

where f_c is an isotropic amplification factor and R_c a chosen "compound anisotropy ratio." The parameters f_c and R_c were obtained by fitting a BEM-derived ECG to an FD-derived ECG, as detailed in Results. The volume conductor for the BEM model is piecewise continuous and isotropic with conductivity σ_B. Conductivity values used in this study are listed in table 1. Details on the two ECG models are given in the following sections.

The underlying V_m were computed by a monodomain reaction-diffusion model of the human heart, as detailed in the next section. The anatomy of the heart and thorax was obtained from in-vivo magnetic resonance imaging data [27].

2.1 propagation model

Propagating action potentials were computed with a monodomain reaction-diffusion model [40, 51]. This model integrated the equation

$$C_\mathrm{m}\frac{\partial V_\mathrm{m}}{\partial t} = \beta^{-1}\nabla\cdot\left(\mathbf{G}(\sigma_\mathrm{mL}, \sigma_\mathrm{mT})\nabla V_\mathrm{m}\right) - I_\mathrm{ion} \tag{6}$$

where β is the membrane surface to volume ratio, C_m is the membrane capacitance per unit area, I_ion the sum of all transmembrane ionic currents, and the equivalent "monodomain" conductivities are defined as $\sigma_\mathrm{mT} = \sigma_\mathrm{iT}\sigma_\mathrm{eT}/(\sigma_\mathrm{iT}+\sigma_\mathrm{eT})$, and $\sigma_\mathrm{mL} = \sigma_\mathrm{iL}\sigma_\mathrm{eL}/(\sigma_\mathrm{iL}+\sigma_\mathrm{eL})$ [40]. Membrane potentials were stored at 1-mm spatial resolution at a 1-ms interval. Each simulation had a duration of 500 ms.

The patient-tailored cardiac anatomy was used for this simulation. Cardiac fiber orientation was mathematically defined as previously described [40]. This procedure was performed at 0.2-mm resolution to obtain smooth fiber orientation profiles. Tissue types and fiber orientations were then subsampled to 1-mm resolution. This subsampled heart model was inserted in the FD torso model, as discussed later on. For the propagation model, which worked at 0.2-mm resolution, each voxel of the subsampled model was replicated 5 times in each spatial dimension, to obtain exactly the same geometry as in the FD torso model.

Because the heart of our patient was relatively large, we assumed that its myocytes were larger than average, and therefore set the surface-to-volume ratio of the cells 20 % smaller than the normal value in our model, to $800\,\mathrm{cm}^{-1}$. This led to realistic activation times.

2.2 BEM model

Previously-described BEM software was used to compute the ECG from the regional dipoles [16, 28, 30, 51]. Briefly, this software uses an integral equation for the potential on the surface triangles due to the regional dipoles. This method, which was first proposed by Barr et al. in 1966 [2, 4], has been used in many studies and is well explained in textbooks [14, 39]. Because this method is well covered in the literature we give only a brief outline here. Details of our implementation can be found in previous publications from our laboratory [28, 30].

Let a set of surfaces S_k bound several regions of continuous isotropic conductivity σ. The notation σ_k^- indicates the conductivity inside surface k, and σ_k^+ the conductivity outside surface k. In one or more of these regions there is a source current density field $\mathbf{J}_\mathrm{c}$ (equation 4). The potential at a point $\mathbf{r}$ on surface k is given by

$$\phi_{ek}(\mathbf{r}) = \frac{1}{2\pi(\sigma_k^- + \sigma_k^+)} \left[\int \mathbf{J}_c(\mathbf{r}') \cdot \frac{\mathbf{r} - \mathbf{r}'}{|\mathbf{r} - \mathbf{r}'|^3} \, dV' + \sum_\ell \int_{S_\ell} (\sigma_\ell^- - \sigma_\ell^+) \, \phi_e(\mathbf{r}'') \, d\Omega_{rr''} \right] \tag{7}$$

where $\mathbf{r}'$ and $\mathbf{r}''$ are variable points, the summation is over all surfaces ℓ, and $d\Omega_{rr''}$ is the solid angle subtended at $\mathbf{r}$ by the infinitesimal surface element situated at $\mathbf{r}''$ [4, 14]. When discretized on a set of triangulated surfaces, this is a system of linear equations for ϕ_e on all surface triangles, with a right-hand side determined by the dipole sources $\mathbf{J}_c$.

The source term $\mathbf{J}_c$ was evaluated at 1-mm resolution according to equation (4) and then integrated over "dipole regions." Except where mentioned otherwise, the heart was divided into $N_d = 29\,689$ dipole regions. Evaluation of $\mathbf{J}_c$ at 1-mm resolution allows the local fiber orientation to be taken into account [53], while the regional integration serves to arrive at a manageable number of sources [28, 51].

Equation (7) was solved (using an iterative method) with a right-hand side in which one of the 3 spatial components of one of the N_d dipoles was set to unity, and all others were set to zero [30]. This process was repeated for every component of every dipole in turn. Each solution yields a set of transfer coefficients that link the dipole component to a contribution to the potential on each of the N_t triangles. Thus, a total of $3N_tN_d$ coefficients link all dipoles to all surface potentials. The coefficients that relate to the outer torso surface triangles were stored and used to compute individual ECGs, while those related to internal surfaces were discarded. In general, the potentials on internal surfaces close to the heart are too inaccurate to be useful, while those on the outer torso surface are highly accurate [14].

The anatomic model, consisting of a set of triangulated surfaces, is shown in figure 1. The torso surface and the inside of the skeletal muscle layer were described by 1216 triangles each. Each lung had ~ 160 triangles, and the intracavitary blood masses ~ 800 triangles. The skeletal muscle layer was represented

using the torso extension method introduced by McFee and Rush [16, 31, 48]. This anisotropic layer with variable fiber orientation, which is assumed to have conductivities 0.43 and 6.67 mS/cm [31, 44], is replaced by a thicker isotropic layer with conductivity 1.25 mS/cm. We used a thickness of 4 cm, which is somewhat more than previously reported [16], because our subject was large and heavily-built. A conductivity $\sigma_B = 2.0$ mS/cm was used for the torso, including the myocardium [16]. Values of σ_B for all regions are listed in table 1.

2.3 FD model

The FD model of the heart and thorax had a resolution of 1 mm and was obtained by scan-converting the surface model of the thorax and inserting the 1-mm version of the heart model. The skeletal muscle layer was represented in the same way as in the BEM model.

From the simulated V_m at 1-mm resolution, $\nabla \cdot (\mathbf{G}_i \nabla V_m)$ was evaluated and used to compute ϕ_e by solving equation (3). This was done using our previously-described software [40] but with 100-fold lower error tolerance levels needed to compute an ECG with < 0.1 mV precision.

2.4 Comparison

The crucial difference between the BEM and FD models is the conductivity of the extracellular space: the BEM model used an isotropic conductivity σ_B, whereas the FD model used anisotropic values σ_{eL} and σ_{eT} (table 1). Our purpose is to try to compensate for the lack of extracellular anisotropy in the BEM model by selecting appropriate values for the constants R_c and f_c.

An analytic solution to this problem exists if both the intracellular and extracellular domain are homogeneous and unbounded [14, 42]. If the coordinate axes

are chosen such that $\mathbf{G}_\mathrm{i}$ and $\mathbf{G}_\mathrm{e}$ are diagonal, equation (3) can be rewritten as

$$\nabla^2 \phi_\mathrm{e} = -\nabla \cdot (\mathbf{G}_\mathrm{c} \nabla V_\mathrm{m}) \tag{8}$$

where

$$\mathbf{G}_\mathrm{c} = \mathbf{G}(\sigma_\mathrm{iL}/(\sigma_\mathrm{iL}+\sigma_\mathrm{eL}), \sigma_\mathrm{iT}/(\sigma_\mathrm{iT}+\sigma_\mathrm{eT})) \tag{9}$$

is also diagonal. The anisotropy ratio of this tensor can be written as

$$R_\mathrm{c} = \frac{\sigma_\mathrm{iL}/(\sigma_\mathrm{iL}+\sigma_\mathrm{eL})}{\sigma_\mathrm{iT}/(\sigma_\mathrm{iT}+\sigma_\mathrm{eT})} = R_\mathrm{i}\frac{\sigma_\mathrm{iT}+\sigma_\mathrm{eT}}{\sigma_\mathrm{iL}+\sigma_\mathrm{eL}} = \frac{R_\mathrm{i}}{R'} \tag{10}$$

where $R' = (\sigma_\mathrm{iL}+\sigma_\mathrm{eL})/(\sigma_\mathrm{iT}+\sigma_\mathrm{eT})$ is the anisotropy ratio of the myocardial bulk conductivity, which opposes the effect of R_i. For the normal conductivity values from table 1, we would have $R_\mathrm{c} = 2.5$ and $R' = 4$.

In case of the heart in situ, the isotropic torso modifies the effect of the bulk myocardial anisotropy. Geselowitz and Miller [12] have discussed an analytic solution for the case of a dipole source in the center of an anisotropic sphere embedded in an unbounded isotropic medium of conductivity σ_0. In this situation, the potential at large distance from the sphere can be reproduced by a homogeneous isotropic medium of conductivity σ_0 if the dipole's transverse and longitudinal components are multiplied by factors f_T and f_L, respectively, given by

$$f_\mathrm{T} = \frac{A\sigma_0}{\sigma_\mathrm{iT}+\sigma_\mathrm{eT}+B\sigma_0} \tag{11}$$

$$f_\mathrm{L} = \frac{A\sigma_0}{\sigma_\mathrm{iL}+\sigma_\mathrm{eL}+B\sigma_0} \tag{12}$$

where $A = 3$ and $B = 2$. If this is a good approximation for the heart in the torso, we should use $f_\mathrm{c} = f_\mathrm{T}$ and $R_\mathrm{c} = R_\mathrm{i}\, f_\mathrm{L}/f_\mathrm{T}$. With the values from table 1, we would now find $R_\mathrm{c} = 5.5$. By analogy with equation (10), we define an effective bulk anisotropy ratio

$$R'_\mathrm{eff} = \frac{R_\mathrm{i}}{R_\mathrm{c}} = \frac{f_\mathrm{T}}{f_\mathrm{L}} \tag{13}$$

which has the value 1.8 in this situation. By comparison with R', we see that the isotropic torso reduces R'_eff, and so amplifies the effect of the intracellular anisotropy of the heart.

Torso boundaries and inhomogeneities also play a role. Thivierge et al. [50] showed that for an anisotropic cube in a bounded isotropic medium, the constants A and B depend on σ_0, on fiber rotation, and on the position of the dipole source in the cube.

Our purpose now is to see how this works out in a complete heart in an inhomogeneous torso, where we identify σ_0 with σ_B for the torso (table 1). Specifically, we will test if values for R_c and $f_c = f_T$ exist that, if applied throughout the heart, still result in an acceptable approximation to the anisotropic ECG. Since we equate f_c and f_T we will from here on refer only to f_T.

We simulated 13 different ECGs with the FD model: a normal activation sequence for several different values of σ_{iL}, σ_{iT}, σ_{eL}, and σ_{eT}; and four abnormal activation sequences with normal conductivity values. In all cases, the propagation model was based on normal conductivity values.

With the BEM model we simulated, for each activation sequence, ECGs for $R_c = 1.0, 1.1, \ldots, 10.0$ and $f_T = 0.1, 0.12, \ldots, 2.0$. For each ECG simulated with the FD model, the BEM ECG with minimal root-mean-square (RMS) difference was selected. RMS and maximum differences were also plotted as functions of (R_c, f_T) to verify the existence of a global minimum. The best choice is reported in terms of its R_c and f_T. We also give f_L, now computed as

$$f_L = f_T R_c / R_i, \tag{14}$$

as well as A and B obtained by inverting the linear system defined by equations (11) and (12), and R'_{eff} (equation 13). Maximum errors and RMS errors are reported, as well as the relative difference (RD) [35, 52], defined as

$$\mathrm{RD} = \sqrt{\frac{\sum_t \sum_n (\phi_{tn}^{\mathrm{BEM}} - \phi_{tn}^{\mathrm{FD}})^2}{\sum_t \sum_n (\phi_{tn}^{\mathrm{FD}})^2}} \tag{15}$$

where the index $t = 1, \ldots, 500$ ranges over all samples, $n = 1, \ldots, 12$ over all leads, ϕ_{tn}^{BEM} is the ECG potential computed with the BEM model, and ϕ_{tn}^{FD} the ECG potential computed with the FD model.

3 Results

3.1 isotropic BEM versus isotropic FD

Ideally, if both the BEM and FD models use isotropic conductivities throughout, they should produce equal results. In practice the results differ slightly because the geometry used in the two models cannot be exactly the same. There were also small differences in the handling of the conductivity tensor in either model. Using $\sigma_{iL} = \sigma_{iT} = 0.66$ mS/cm and $\sigma_{eL} = \sigma_{eT} = \sigma_0 = 2.0$ mS/cm in both models, we found an RMS difference of 34 μV, a maximum difference of 273 μV, and RD $= 0.08$, for a BEM model with 29689 dipoles.

With 5004 dipoles in the BEM model, the difference was slightly larger: 315 μV max, 42 μV RMS, RD $= 0.10$.

With 88 dipoles in the BEM model as in previous work [28, 51], the difference between isotropic BEM and FD models was 577 μV max, 99 μV RMS, RD $=$ 0.23.

3.2 anisotropic BEM versus anisotropic FD

Simulations were performed for sinus rhythm and four abnormal activation sequences, each initiated by stimulating a single site in the ventricular myocardium: “apex” = epicardially in the left ventricular (LV) apex, “LV epi” = in the LV free wall epicardium near the base of the anterior papillary muscle, “LV endo” = endocardially at the same site, and “RV endo” = in the right ventricular (RV) endocardium near the RV anterior papillary muscle. The sinus rhythm simulation was repeated with 8 different conductivity settings for the ventricular myocardium. Values of R_c and f_T were determined that gave an optimal match between BEM and FD models in a least-squares sense.

The results of the sinus rhythm simulations are listed in table 2. For normal conductivity values, RMS and maximum errors (difference between BEM and FD results) were 46 and 354 μV, respectively. This was achieved with $R_c = 5.8$ for the BEM model. Corresponding parameters according to Geselowitz and Miller [12, 50] are $A = 4.2$ (ideally 3) and $B = 2.4$ (ideally 2). The anisotropy of the bulk myocardium thus had the effect of amplifying the transverse components of the dipoles by a factor $f_T = 1.36$ and diminishing the longitudinal component by a factor $f_L = 0.79$.

When conductivity values were varied, the optimal settings to match BEM and FD results varied as well. Optimal R_c ranged from 3.4 to 7.6. Nevertheless, RMS errors were acceptable in all cases (at most 77 μV). Maximum errors of up to 530 μV (5 mm on standard ECG paper) may seem unacceptable, but these occurred always at the peak of ECG deflections, with amplitudes of up to 2 mV, and represented a relative error in the order of 25 %. Overall RD values ≤ 0.17 also indicate a good match.

For practical application of the BEM, predetermined values of R_c and f_T should be usable for different activation sequences. This is tested in table 3. Optimal values of R_c and f_T were determined for a normal activation sequence, and applied to ectopic beats. For the abnormal activation sequences this leads to doubled RMS errors, but not to an increase in maximum errors. The relatively large errors for the apically paced sequence are due to the large signal amplitudes it generates; its RD is relatively low.

When only 88 instead of 29689 dipole sources were used, the difference between the BEM and FD models for the normal activation sequence (top row in table 3) increased slightly to 59 μV RMS; RD = 0.16, while the maximum error decreased to 262 μV. This indicates that the number of dipoles is not very important, even for an anisotropic BEM model.

3.3 isotropic BEM versus anisotropic FD

An important practical question is whether a BEM should be used with isotropic or anisotropic conductivity [14, 50]. Therefore we also compared isotropic BEM results with anisotropic FD results. With fixed $R_c = 1$ we found that the optimal f_T for the normal activation sequence was 1.50. With these values we simulated the ECGs for the abnormal activation sequences. Results are shown in table 4. RMS errors are now 3 to 5 times larger than with the anisotropic BEM, and maximum errors are well above 1 mV. RD values also indicate a bad match.

3.4 only intracellular anisotropy

Some previous studies have used BEM models in which only intracellular anisotropy was represented, with an anisotropy ratio 9 [20, 53]. We compared the result of such settings with an FD model in which $R_i = 10$, as before. With fixed $R_c = 9$ we found that the optimal f_T for the normal activation sequence was 1.01. With these values we simulated the ECGs for the abnormal activation sequences. Results are shown in table 5. RMS errors and RD are considerably larger than in the BEM model with $R_c = 5.8$, but not as large as in the fully isotropic model.

3.5 qualitative comparison

The main results are repeated in figure 2 to allow a qualitative comparison of BEM and FD results. In each panel, an ECG simulated with the BEM model (black) is printed superposed on an ECG simulated with the FD model (gray). The two simulations are hardly distinguishable in the isotropic case. Small differences on the peaks of the T waves can be observed when anisotropic models are compared. In contrast, an isotropic model compared to an anisotropic model shows a different

progression of R/S waves through the precordial leads (only V1, V3 and V5 are shown).

4 Discussion

This study demonstrates that ECGs computed with a BEM model closely resemble those computed with an anisotropic FD model if a suitable compound anisotropy (R_c) and scaling factor (f_T) are used. We found $R_c \approx 6$. Although optimal parameters R_c and f_T have to be found experimentally for a given set of heart and torso conductivities, and perhaps also depend on the torso anatomy, they can be used for different activation sequences. Thus, one comparison with an FD model suffices to gauge a given BEM model.

The perceived impossibility of representing extracellular anisotropy in a BEM model has caused previous authors to take two different approaches: fully isotropic models [1, 28, 32] and models that represented intracellular anisotropy only [20, 53]. Our study shows that there is no need for such extreme positions, because an intermediate value of R_c results in a very accurate representation of the two anisotropies. The use of intracellular anisotropy alone gave better results than full isotropy, but the best results were obtained with an intermediate value.

In general, anisotropy cannot be neglected in forward ECG simulation [15, 29, 33, 50, 53]. We found differences between isotropic and anisotropic models primarily in the precordial leads V1 to V5. Difficulties with leads V3–V5 can be observed in studies that used fully isotropic models [45], and in others were probably hidden because activation sequences and heart orientation were, especially in older studies, often adapted to improve the ECG.

4.1 role of intracellular and extracellular conductivities

The results in table 2 show that the effect of the torso and the four intracellular and extracellular conductivities on the surface ECG can be approximated with a single compound anisotropy ratio R_c and an amplification factor f_T. As expected, larger R_i led to larger R_c, and larger R_e led to smaller R_c. These relations were nonlinear.

The normal value $R_c = 5.8$ was much larger than what would be expected for an unbounded homogeneous myocardium (2.5) but similar to the value expected for an anisotropic sphere embedded in an unbounded isotropic medium (5.5). This similarity is probably coincidental, since it only occurred for the normal set of conductivities. Moreover, the anisotropic-sphere approximation did not accurately predict f_T.

As expected, higher extracellular conductivity led to smaller ECG signals (smaller f_T), and higher intracellular conductivity to larger ECG signals (larger f_T). These relationships were nonlinear.

Differences between the FD model and the anisotropic BEM model (table 3) depended on the activation sequence. This may be due to the variable importance of propagation along the fibers in different activation sequences.

4.2 modeling techniques

Application of the most efficient numerical techniques was not a priority in this study. Our FD model based on a regular mesh with 1-mm resolution ensured sufficient accuracy, but is far from efficient. We chose this method for practical reasons only and do not recommend its application in general. A more efficient approach is a finite-element (FE) discretization of the heart, coupled with a BEM model of the torso [5, 10] or as an integrated part of an FE torso model [26]. Regular FD meshes of the torso at lower resolutions than our 1 mm have also been reported [22–24, 54].

Similarly, a BEM model with nearly 30 thousand dipole sources is not useful in all BEM applications. We used this large number to minimize bias due to systematic errors. Comparisons with a BEM model using only 88 dipoles, the number we used in previous work [28, 51], showed a small increase in RMS error. Interestingly, an isotropic model seemed to be more sensitive to a small number of

dipoles than an anisotropic model. This may be explained by the greater influence of transmural dipole components in the isotropic model. This component is most affected by the error introduced by spatial averaging in large dipole regions.

Thus, the ability of the BEM model with dipole sources to deal with anisotropy does not rely on a large number of dipoles. It depends only on the evaluation of $\mathbf{J}_c$ (equation 4) on a scale that is small enough to account for local fiber orientation. The effect of the regional integration of $\mathbf{J}_c$, which is done to arrive at a reasonable number of dipoles to place in the BEM model, is to approximate the locations of all “small” dipoles in a region by the location of the “large” dipole. The effect of this approximation on the ECG is negligible.

4.3 related studies

In the limited space of a research paper we cannot do justice to all the work that has been done on forward ECG simulation. Several good reviews [13, 17, 34] and textbooks treat this subject in depth. Here, we give a limited account of the discussion on anisotropic forward models and the accuracy of BEM models.

Several authors have discussed the relative merits of integral equations discretized with the BEM on the one hand, and differential equations discretized with FD/finite-element (FE) methods on the other [38, 41, 46, 49]. However, these studies addressed the relation between torso surface potentials and cardiac surface potentials – a very different source model than ours. With epicardial potentials as a source model, anisotropy cannot be accounted for at all. The same is true for equivalent double layer models [11, 35, 36], in which the source consists of (equivalent) membrane potentials on the myocardial surface. With some notable exceptions [37], these source models are mostly used for inverse models, where anisotropy is deemed less important than in forward ECG models [33].

As discussed above, the situation is different when current dipole sources throughout the cardiac volume are used. If these are evaluated at high spatial resolution, e.g. 1-mm^3 volumes in our study, inhomogeneous intracellular anisotropy can easily be taken care of (equation 4), as shown, for example, by Wei et al. [53]. Hren et al. [20] named this an "oblique dipole model." Representing intracellular anisotropy and neglecting extracellular anisotropy would result in exaggerated anisotropic effects [14, 50], so the relevant questions that remained were whether extracellular anisotropy can be accounted for, and whether this improves the ECG. Our answer to both questions is affirmative. These conclusions, obtained here with a model based on volume-averaged current dipoles, may also apply to the oblique dipole layer model [6, 7]. Such an approach has in fact been used by Roberts and Scher [42], with analytically-derived f_T and f_L for a spheroidal wave front, to simulate ϕ_e inside the heart muscle.

4.4 inhomogeneities

A remaining limitation of BEM methods is that they cannot treat inhomogeneous conductivity as easily as FD and FE methods. In our study, the heart was anisotropic with inhomogeneous fiber orientation, but the longitudinal and transverse conductivities were the same throughout the myocardium. It is not clear whether an area with different conductivity parameters could be treated in a BEM model by assigning other values for the parameters R_c and f_T in this area. It could be necessary to assign a boundary around such an area. Inhomogeneity plays a role when, for example, hypertrophy, cardiomyopathy, or an advanced state of myocardial ischemia or infarction is modeled.

4.5 Conclusion

We conclude that not only intracellular, but also extracellular anisotropy can be implemented in current dipole-based BEM models for the ECG, and that representing both anisotropies improves the accuracy of the simulated ECG. As a rule of thumb, a compound anisotropy ratio of 6 can be used.

Acknowledgements The authors would like to thank Dr. André Linnenbank and Dr. Pieter Postema from the University of Amsterdam for providing the heart-torso anatomy, and Dr. Adriaan van Oosterom from the Centre Hospitalier Universitaire Vaudois, Lausanne, for his valuable suggestions and comments.

References

1. Aoki M, Okamoto Y, Musha T, Harumi KI (1987) Three-dimensional simulation of the ventricular depolarization and repolarization processes and body surface potentials: Normal heart and bundle branch block. IEEE Trans Biomed Eng 34(6):454–462
2. Barnard AC, Duck IM, Lynn MS (1967) The application of electromagnetic theory to electrocardiology; I. derivation of the integral equations. Biophys J 7:443–462
3. Barnard AC, Duck IM, Lynn MS, Timlake WP (1967) The application of electromagnetic theory to electrocardiology; II. numerical solution of the integral equations. Biophys J 7:463–490
4. Barr RC, Pilkington TC, Boineau JP, Spach MS (1966) Determining surface potentials from current dipoles, with application to electrocardiography. IEEE Trans Biomed Eng 13(2):88–92
5. Buist M, Pullan A (2002) Torso coupling techniques for the forward problem of electrophysiology. Ann Biomed Eng 30:1299–1312
6. Colli-Franzone P, Guerri L, Viganotti C, Macchi E, Baruffi S, Spaggiari S, Taccardi B (1982) Potential fields generated by oblique dipole layers modeling excitation wavefronts in the anisotropic myocardium; comparison with potential fields elicited by paced dog hearts in a volume conductor. Circ Res 51(3):330–346
7. Colli-Franzone P, Guerri L, Viganotti C (1983) Oblique dipole layer potentials applied to electrocardiology. J Math Biol 17:93–124

8. Colli Franzone P, Guerri L, Pennacchio M, Taccardi B (2000) Anisotropic mechanisms for multiphasic unipolar electrograms: Simulation studies and experimental recordings. Ann Biomed Eng 28:1326–1342
9. van Dam PM, Oostendorp TF, van Oosterom A (2008) Application of the fastest route algorithm in the interactive simulation of the effect of local ischemia on the ECG. Med & Biol Eng & Comput 47:11–20
10. Fischer G, Tilg B, Modre R, Huiskamp GJM, Fetzer J, Rucker W, Wach P (2000) A bidomain model based BEM-FEM coupling formulation for anisotropic cardiac tissue. Ann Biomed Eng 28:1229–1243
11. Geselowitz DB (1989) On the theory of the electrocardiogram. Proc IEEE 77(6):857–876
12. Geselowitz DB, Miller WT III (1983) A bidomain model for anisotropic cardiac muscle. Ann Biomed Eng 11:191–206
13. Gulrajani RM (1988) Models of the electrical activity of the heart and computer simulation of the electrocardiogram. CRC Critical Reviews in Biomedical Engineering 16(1):1–66
14. Gulrajani RM (1998) Bioelectricity and Biomagnetism. Wiley, New York, NY
15. Gulrajani RM, Lorange M (1986) Simulation of myocardial anisotropy effects on the ECG. In: Kondraske GV, Robinson CJ (eds) Proc. 8th Ann. Conf. IEEE-EMBS, p 358
16. Gulrajani RM, Mailloux GE (1983) A simulation study of the effects of torso inhomogeneities on electrocardiographic potentials, using realistic heart and torso models. Circ Res 52:45–56
17. Gulrajani RM, Roberge FA, Mailloux GE (1989) The forward problem of electrocardiography. In: Macfarlane PW, Lawrie TDV (eds) Comprehensive Electrocardiology, vol 1, Pergamon Press, chap 8
18. Henriquez CS (1993) Simulating the electrical behavior of cardiac tissue using the bidomain model. CRC Crit Rev Biomed Eng 21:1–77
19. Horacek BM (1973) Digital model for studies in magnetocardiography. IEEE Trans Magn 3:440–444
20. Hren R, Nenonen J, Horáček BM (1998) Simulated epicardial potential maps during paced activation reflect myocardial fibrous structure. Ann Biomed Eng 26:1–14
21. Huiskamp G (1998) Simulation of depolarization in a membrane-equations-based model of the anisotropic ventricle. IEEE Trans Biomed Eng 45(7):847–855
22. Hyttinen J, Viik J, Lehtinen R, Plonsey R, Malmivuo J (1997) Computer model analysis of the relationship of ST-segment and ST-segment/heart rate slope response to the constituents of the ischemic injury source. J Electrocardiol 30(3):161–174

23. Kauppinen P, Hyttinen J, Laarne P, Malmivuo J (1999) A software implementation for detailed volume conductor modelling in electrophysiology using finite difference method. Computer Meth & Prog in Biomedicine 58:191–203
24. Keller DUJ, Seemann G, Weiss DL, Farina D, Zehelein J, Dössel O (2007) Computer based modeling of the congenital long-QT 2 syndrome in the Visible Man torso: From genes to ECG. In: Proc. 29th Annu. Int. Conf. IEEE EMBS, Lyon, France, pp 1410–1413
25. Lines GT, Buist ML, Grøttum P, Pullan AJ, Sundnes J, Tveito A (2003) Mathematical models and numerical methods for the forward problem in cardiac electrophysiology. Comput Visual Sci 5:215–239
26. Lines GT, Grøttum P, Tveito A (2003) Modeling the electrical activity of the heart; A bidomain model of the ventricles embedded in a torso. Comput Visual Sci 5:195–213
27. Linnenbank AC, van Oosterom A, Oostendorp T, van Dessel PFHM, van Rossum AC, Coronel R, Tan HL, de Bakker JMT (2006) Non-invasive imaging of activation times during drug-induced conduction changes. In: World Congress on Medical Physics and Biomedical Engineering, IFMBE, Seoul
28. Lorange M, Gulrajani RM (1993) A computer heart model incorporating anisotropic propagation: I. Model construction and simulation of normal activation. J Electrocardiol 26(4):245–261
29. MacLachlan MC, Sundnes J, Lines GT (2005) Simulation of ST segment changes during subendocardial ischemia using a realistic 3-D cardiac geometry. IEEE Trans Biomed Eng 52(5):799–807
30. Mailloux GE, Gulrajani RM (1982) Theoretical evaluation of the McFee and Frank vectorcardiographic lead systems using a numerical inhomogeneous torso model. IEEE Trans Biomed Eng 29(5):322–332
31. McFee R, Rush S (1968) Qualitative effects of thoracic resistivity variations on the interpretation of electrocardiograms: The low resistance surface layer. Am Heart J 76(1):48–61
32. Miller WT III, Geselowitz DB (1978) Simulation studies of the electrocardiogram; I. The normal heart. Circ Res 43(2):301–315
33. Modre R, Seger M, Fischer G, Hintermüller C, Hayn D, Pfeifer B, Hanser F, Schreier G, Tilg B (2006) Cardiac anisotropy: Is it negligible regarding noninvasive activation time imaging? IEEE Trans Biomed Eng 53(4):569–580
34. van Oosterom A (1997) Forward and inverse problems in electrocardiography. In: Panfilov AV, Holden AV (eds) Computational Biology of the Heart, Wiley, chap 11, pp 295–343

35. van Oosterom A (2001) Genesis of the T wave as based on an equivalent surface source model. J Electrocardiol 34 Suppl.:217–227
36. van Oosterom A, Jacquemet V (2005) Genesis of the P wave: Atrial signals as generated by the equivalent double layer source model. Europace 7 Suppl 2:S21–S20
37. van Oosterom A, Oostendorp TF (2004) ECGSIM: an interactive tool for simulating QRST waveforms. Heart 90:165–168
38. Pilkington TC, Morrow MN, Stanley PC (1987) A comparison of finite element and integral equation formulations for the calculation of electrocardiographic potentials–II. IEEE Trans Biomed Eng 34(3):258–260
39. Plonsey R, Fleming D (1969) Bioelectric Phenomena. McGraw-Hill, New York
40. Potse M, Dubé B, Richer J, Vinet A, Gulrajani RM (2006) A comparison of monodomain and bidomain reaction-diffusion models for action potential propagation in the human heart. IEEE Trans Biomed Eng 53(12):2425–2435
41. Pullan A (1996) A high-order coupled finite element/boundary element torso model. IEEE Trans Biomed Eng 43:292–298
42. Roberts DE, Scher AM (1982) Effect of tissue anisotropy on extracellular potential fields in canine myocardium in situ. Circ Res 50:342–351
43. Roth BJ (1997) Electrical conductivity values used with the bidomain model of cardiac tissue. IEEE Trans Biomed Eng 44:326–328
44. Rush S, Nelson CV (1976) The effects of electrical inhomogeneity and anisotropy of thoracic tissues on the field of the heart. In: Nelson CV, Geselowitz DB (eds) The Theoretical Basis of Electrocardiology, Clarendon, Oxford, pp 323–354
45. Rush S, Lux R, Baldwin A, Lepeschkin E (1980) Quantitative comparison of pre-mortem ECG's with those reconstructed from activation data of a revived heart. J Electrocardiol 13(3):275–282
46. Seger M, Fischer G, Modre R, Messnarz B, Hanser F, Tilg B (2005) Lead field computation for the electrocardiographic inverse problem—finite elements versus boundary elements. Computer Meth & Prog in Biomedicine 77:241–252
47. Shou G, Xia L, Jiang M, Wei Q, Liu F, Crozier S (2008) Truncated total least squares: A new regularization method for the solution of ECG inverse problems. IEEE Trans Biomed Eng 55(4):1327–1355
48. Stanley PC, Pilkington TC, Morrow MN, Ideker RE (1991) An assessment of variable thickness and fiber orientation of the skeletal muscle layer on electrocardiographic calculations. IEEE Trans Biomed Eng 38(11):1069–1076

49. Stenroos M, Haueisen J (2008) Boundary element computations in the forward and inverse problems of electrocardiography: Comparison of collocation and Galerking weightings. IEEE Trans Biomed Eng 55(9):2124–2133

50. Thivierge M, Gulrajani RM, Savard P (1997) Effects of rotational myocardial anisotropy in forward potential computations with equivalent heart dipoles. Ann Biomed Eng 25(3):477–498

51. Trudel MC, Dubé B, Potse M, Gulrajani RM, Leon LJ (2004) Simulation of propagation in a membrane-based computer heart model with parallel processing. IEEE Trans Biomed Eng 51(8):1319–1329

52. Tyšler M, Kneppo P, Turzová M, Švehlíková J, Karas S, Hebláková E, Hána K, Filipová S (2007) Noninvasive assessment of local myocardium repolarization changes using high resolution surface ECG mapping. Physiol Res 56 Suppl. 1:S133–S141

53. Wei D, Okazaki O, Harumi K, Harasawa E, Hosaka H (1995) Comparative simulation of excitation and body surface electrocardiogram with isotropic and anisotropic computer heart models. IEEE Trans Biomed Eng 42(4):343–357

54. Wei Q, Liu F, Appleton B, Xia L, Liu N, Wilson S, Riley R, Strugnel W, Slaughter R, Denman R, Crozier S (2006) Effect of cardiac motion on body surface electrocardiographic potentials: an MRI-based simulation study. Phys Med Biol 51:3405–3418

55. Zhu X, Wei D (2007) Computer simulation of intracardiac potential with whole-heart model. Int J Bioinf Res App 3:100–122

Table 1 Tissue conductivity values

material	source	σ_{iT}	σ_{iL}	R_i	σ_{eT}	σ_{eL}	R_e	σ_B
ventricular muscle	[43]	0.30	3.00	10	1.20	3.00	2.5	2.00
body	[31]	0	0		2.00	2.00	1	2.00
blood	[31]	0	0		6.00	6.00	1	6.00
lung	[31]	0	0		0.50	0.50	1	0.50
skeletal muscle[1]	[31]	0	0		1.25	1.25	1	1.25
air	[31]	0	0		0	0		0

[1]value adapted for treatment of anisotropy; see text.

Units are mS/cm. “source” = literature reference.

Table 2 Anisotropic BEM with optimal settings compared to anisotropic FD.

	conductivity (mS/cm)						error (μV)								
sequence	σ_{iL}	σ_{iT}	σ_{eL}	σ_{eT}	R_i	R_e	rms	max	RD	R_c	f_T	f_L	A	B	R'_{eff}
normal	3.00	0.30	3.00	1.20	10	2.5	46	354	0.13	5.80	1.36	0.79	4.2	2.4	1.7
normal	3.00	0.30	**1.50**	**0.60**	10	2.5	77	340	0.17	3.80	1.98	0.75	2.2	0.7	2.6
normal	3.00	0.30	**4.50**	**1.80**	10	2.5	50	352	0.16	7.20	1.06	0.76	7.3	5.9	1.4
normal	**1.50**	**0.15**	3.00	1.20	10	2.5	25	171	0.13	5.60	0.75	0.42	1.5	1.3	1.8
normal	**4.50**	**0.45**	3.00	1.20	10	2.5	68	530	0.14	5.80	1.89	1.10	7.6	3.2	1.7
normal	3.00	0.30	3.00	**0.60**	10	5.0	74	361	0.17	3.40	1.98	0.67	2.6	0.9	2.9
normal	3.00	0.30	3.00	**1.80**	10	1.7	50	347	0.15	7.60	1.06	0.80	6.5	5.1	1.3
normal	3.00	0.30	**1.50**	1.20	10	1.2	47	346	0.12	6.20	1.36	0.85	3.3	1.7	1.6
normal	3.00	0.30	**4.50**	1.20	10	3.8	46	359	0.13	5.20	1.36	0.71	4.4	2.5	1.9

σ_{iL}, σ_{iT}, σ_{eL} and σ_{eT} are the conductivities used by the FD model. error = difference between BEM and FD simulated ECGs. normal = sinus rhythm. Bold type is used to highlight abnormal conductivity settings.

Table 3 Anisotropic BEM with fixed R_c and f_T compared to anisotropic FD.

	conductivity (mS/cm)						error (μV)								
sequence	σ_{iL}	σ_{iT}	σ_{eL}	σ_{eT}	R_i	R_e	rms	max	RD	R_c	f_T	f_L	A	B	R'_{eff}
normal	3.00	0.30	3.00	1.20	10	2.5	46	354	0.13	**5.80**	**1.36**	0.79	4.2	2.4	1.7
LV apex	3.00	0.30	3.00	1.20	10	2.5	115	221	0.10	**5.80**	**1.36**	0.79	4.2	2.4	1.7
LV epi	3.00	0.30	3.00	1.20	10	2.5	80	374	0.11	**5.80**	**1.36**	0.79	4.2	2.4	1.7
LV endo	3.00	0.30	3.00	1.20	10	2.5	76	322	0.14	**5.80**	**1.36**	0.79	4.2	2.4	1.7
RV endo	3.00	0.30	3.00	1.20	10	2.5	85	423	0.10	**5.80**	**1.36**	0.79	4.2	2.4	1.7

Bold type is used to highlight newly fixed parameter settings. apex = apical stimulation (see text). endo/epi = endocardial/epicardial stimulation (see text). Other abbreviations are as in table 2.

Table 4 Isotropic BEM compared to anisotropic FD.

	conductivity (mS/cm)						error (μV)								
sequence	σ_{iL}	σ_{iT}	σ_{eL}	σ_{eT}	R_i	R_e	rms	max	RD	R_c	f_T	f_L	A	B	R'_{eff}
normal	3.00	0.30	3.00	1.20	10	2.5	211	1833	0.59	**1.00**	**1.50**	0.15	–	–	10
LV apex	3.00	0.30	3.00	1.20	10	2.5	401	1579	0.34	**1.00**	**1.50**	0.15	–	–	10
LV epi	3.00	0.30	3.00	1.20	10	2.5	393	1213	0.54	**1.00**	**1.50**	0.15	–	–	10
LV endo	3.00	0.30	3.00	1.20	10	2.5	367	1239	0.65	**1.00**	**1.50**	0.15	–	–	10
RV endo	3.00	0.30	3.00	1.20	10	2.5	447	1815	0.53	**1.00**	**1.50**	0.15	–	–	10

Bold type is used to highlight newly fixed parameter settings. Abbreviations are as in tables 2 and 3.

Table 5 BEM with only intracellular anisotropy compared to anisotropic FD.

	conductivity (mS/cm)						error (μV)								
sequence	σ_{iL}	σ_{iT}	σ_{eL}	σ_{eT}	R_i	R_e	rms	max	RD	R_c	f_T	f_L	A	B	R'_{eff}
normal	3.00	0.30	3.00	1.20	10	2.5	95	238	0.26	**9.00**	**1.01**	0.91	–	–	1.1
LV apex	3.00	0.30	3.00	1.20	10	2.5	113	264	0.10	**9.00**	**1.01**	0.91	–	–	1.1
LV epi	3.00	0.30	3.00	1.20	10	2.5	126	423	0.17	**9.00**	**1.01**	0.91	–	–	1.1
LV endo	3.00	0.30	3.00	1.20	10	2.5	155	489	0.28	**9.00**	**1.01**	0.91	–	–	1.1
RV endo	3.00	0.30	3.00	1.20	10	2.5	155	799	0.18	**9.00**	**1.01**	0.91	–	–	1.1

Bold type is used to highlight newly fixed parameter settings. Abbreviations are as in tables 2 and 3.

Figure Captions

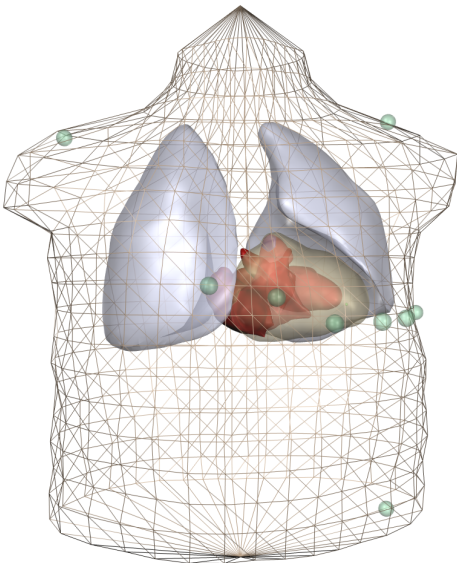

Fig. 1 Anatomic model. The triangulation of the torso corresponds to that used in the BEM model. For clarity, other components are shown as smooth surfaces. The standard ECG electrodes (three limb electrodes and six precordial electrodes) are shown as green spheres. For actual simulations the torso surface was replaced by inner and outer surfaces of the skeletal muscle layer, and electrodes moved to the outer layer.

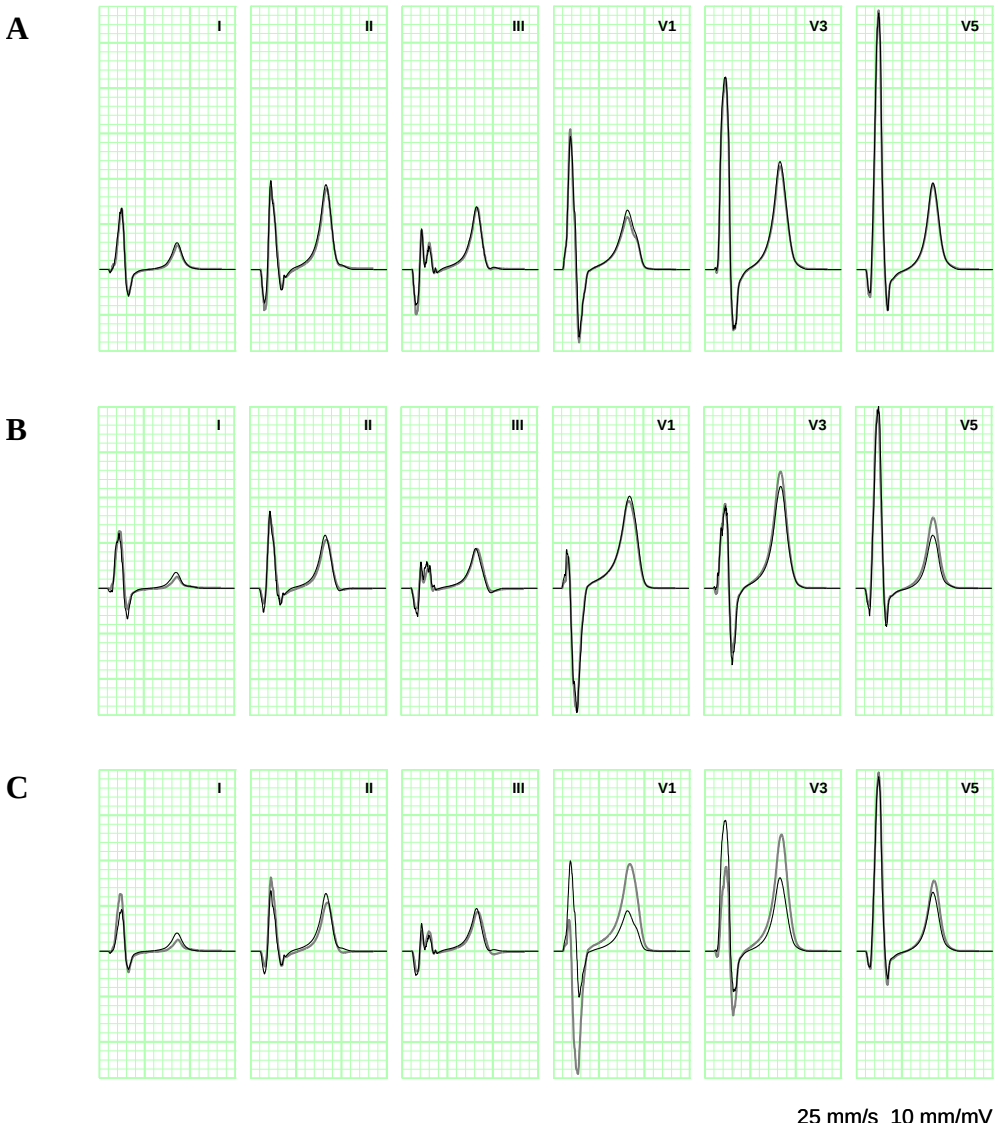

Fig. 2 Comparison of ECGs simulated with an FD model (gray) and with a BEM model (black). ECGs were obtained from a normal (sinus rhythm) activation sequence. A representative subset of the standard 12-lead ECG is shown. ECGs are displayed in the conventional way, using grid lines with 40 ms spacing horizontally and 0.1 mV spacing vertically, and no axis labels. **A:** both models isotropic (RD = 0.08). **B:** both models anisotropic (RD = 0.13, table 3). **C:** fully isotropic BEM versus anisotropic FD model (RD = 0.59, table 4).